ACS OMEGA

http://pubs.acs.org/journal/acsodf

Article

Integrational Technologies for the Development of Three-Dimensional Scaffolds as Platforms in Cartilage Tissue Engineering

Nimrah Munir, Alison McDonald, and Anthony Callanan*

Cite This: *ACS Omega* 2020, 5, 12623−12636

Read Online

ACCESS | Metrics & More | Article Recommendations

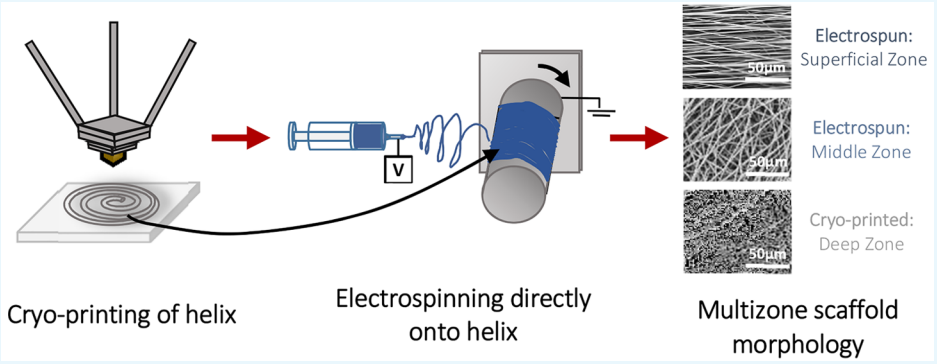

ABSTRACT: The prevalence of osteoarthritis is on the rise, and an effective treatment for cartilage defects is still being sought. Cartilage tissue *in vivo* encompasses complex structures and composition, both of which influence cells and many properties of the native cartilage. The extracellular matrix structure and components provides both morphological cues and the necessary signals to promote cell functions including metabolism, proliferation, and differentiation. In the present study, cryo-printing and electrospinning were combined to produce multizone scaffolds that consist of three distinctive zones. These scaffolds successfully mimic the collagen fiber orientation of the native cartilage. Moreover, *in vitro* analysis of chondrocyte-seeded scaffolds demonstrated the ability of multizone scaffolds to support long-term chondrocyte attachment and survival over a 5 week culture period. Moreover, multizone scaffolds were found to regulate the expression of key genes in comparison to the controls and allowed the detection of sulfated glycosaminoglycan. Evaluation of the compressive properties revealed that the multizone scaffolds possess more suitable mechanical properties, for the native cartilage, in comparison to the electrospun and phase-separated controls. Multizone scaffolds provide viable initial platforms that capture the complex structure and compressive properties of the native cartilage. They also maintain chondrocyte phenotype and function, highlighting their potential in cartilage tissue engineering applications.

INTRODUCTION

Cartilage is an avascular tissue characterized with a largely senescent cell population and has limited ability for self-repair in response to damage. Due to this, the treatment of cartilage-related degenerative disorders has proven to be a challenge.[1−3] The rise in aging population has indicated increased prevalence of degenerative musculoskeletal diseases including osteoarthritis.[4,5] Despite the advancement of surgical techniques and the utilization of modified grafting, the incidence of osteoarthritis is projected to increase;[6−8] thus, new and effective treatments are required.

Cartilage tissue engineering is an emerging promising approach to repair and potentially restore articular defects resulting from cartilage damage, osteoarthritis, and other degenerative joint diseases.[9] Advancements in scaffold materials and fabrication techniques have provided an insight into the influence of scaffold microstructure and composition on chondrocyte growth, viability, and its ability to produce the extracellular matrix (ECM).[10−19] Electrospun scaffolds have gained widespread attention as their structure mimics the dimensions of the ECM and is capable of promoting cell attachment and proliferation.[20−24] While electrospinning has the ability to precisely form continuous and highly organized fibers, often achieving adequate compressive properties, especially for load-bearing tissues including cartilage, is a challenge.[22,25,26]

On the other hand, rapid prototype techniques, including 3D printing, allow great control over scaffold mechanical

Received: November 26, 2019
Accepted: May 5, 2020
Published: May 27, 2020

https://dx.doi.org/10.1021/acsomega.9b04022
ACS Omega 2020, 5, 12623−12636

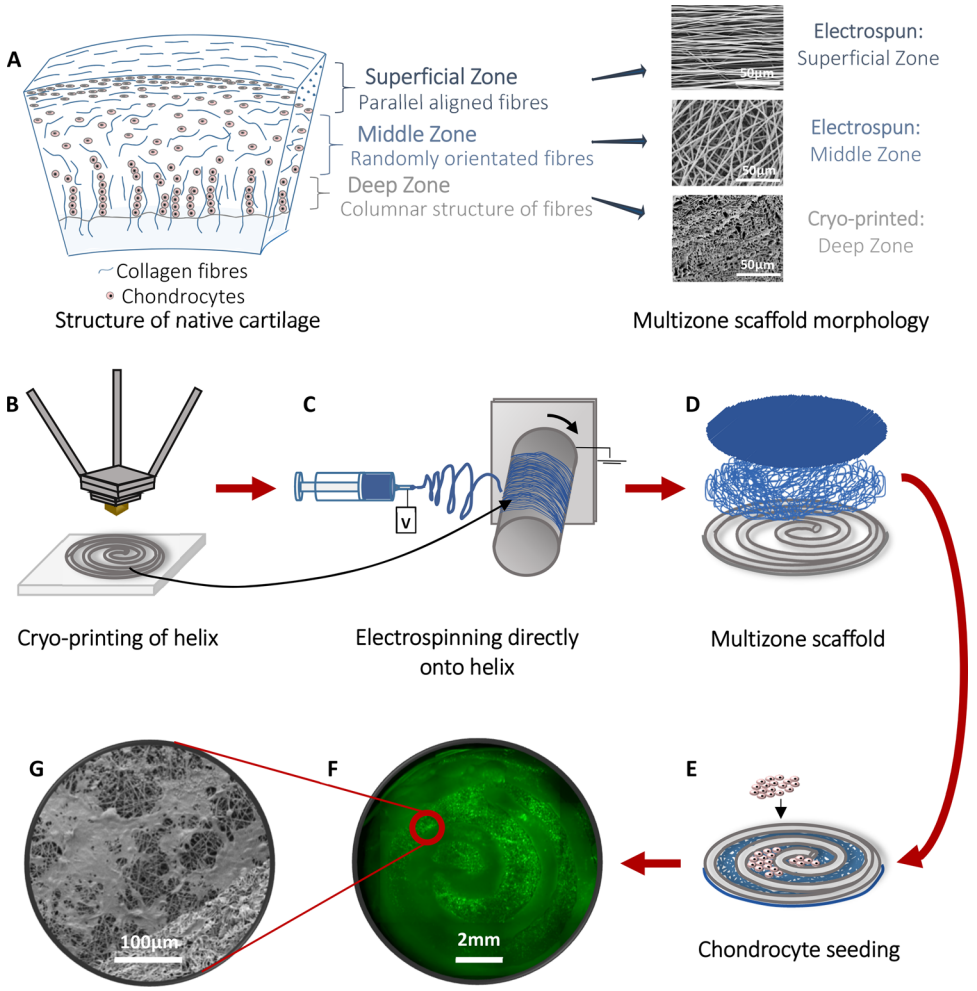

Figure 1. Schematic of the cartilage and scaffold design and methods used to fabricate multizone scaffolds and cell seeding. (A) Structure of the native cartilage and morphology of the zones of the multizone scaffold. (B) Cryo-printing of helix for the bottom layer of the multizone scaffold. (C) Electrospinning random and aligned fibers directly on to the printed helix. (D) The multizone scaffold has three distinctive zones each, which mimics the collagen fiber orientation of collagen fibers in the native cartilage. (E) Chondrocytes are seeded into the void of the cryo-printed helix, directly onto the electrospun fibers. (F) Epifluorescence image of the multizone scaffold showing chondrocyte localization in the void of the cryo-printed helix layer and on top of the electrospun layers after 24 h of culture. Chondrocytes stained with phalloidin. (G) SEM image of chondrocyte-seeded multizone scaffolds showing cell attachment after 24 h of culture. Chondrocytes were stained with osmium.

properties as well as porosity and interconnectivity. Advances in rapid prototype techniques have opened up the avenue of allowing scaffolds to be designed accordingly to match tissue-specific properties.[27] Specifically, cryo-printing, a scaffold fabrication technique that incorporates 3D printing and directional freezing, allows the production of highly porous scaffolds with tailorable pore size, porosity, and mechanical properties.[28,29] Although rapid prototype techniques offer many advantages of use, limited resolution, pore size, and material selection hinder their potential in tissue regeneration applications.[26] Complex 3D structures, enhanced pore size, and mechanical properties can be achieved through the integration of rapid prototype techniques with electrospinning.[30−33] However, none have investigated the combination of cryo-printing and electrospinning for producing scaffolds for cartilage tissue engineering applications.

Given the distinctive structural and composition differences between the various layers of the native cartilage, hybrid scaffolds, which take these into consideration, are being sought.[34,35] Indeed, while cells isolated from the different zones of the cartilage have been seeded into scaffolds to create zonal differences,[36] the isolation of cells from individual zones has proven to be difficult. There is a growing interest toward developing scaffolds that account for these zonal architecture differences. Such multilayered scaffolds have been recently developed using phase separation and directional freezing, which involve directional ice crystal nucleation that allows the production of unidirectional pores.[37,38] Another approach to mimic the zonal pore differences in the cartilage is through the production of gradient scaffolds.[39,40] Previous zonal constructs have investigated pore size variations, material selection,[41] zonal cell isolation,[39,40] and architecture variations.[11,42] However, there is a lack of research on multilayered scaffolds that consider collagen fiber orientation and compressive properties.

In order to capture the zonal architecture and mechanical properties of the native cartilage, the present study developed multizone scaffolds through the integration of various scaffold fabrication methodologies including cryo-printing and electrospinning. Additionally, to capture the *in vitro* cellurization procedure, which is employed in autologous chondrocyte implantation (ACI), we examined cell populations that have

https://dx.doi.org/10.1021/acsomega.9b04022
ACS Omega 2020, 5, 12623−12636

undergone a higher number of doublings such as that used clinically.[43,44] The multizone scaffold is composed of three different zones. The bottom layer of the multizone scaffold consists of a cryo-printed helix, made using cryo-printing, which represents the deep zone of the cartilage and is responsible for the mechanical properties. The middle and top zones are fabricated using electrospinning. Both randomly orientated and highly aligned fibers were deposited directly onto the cryo-printed helix to represent the middle and superficial zone of the native cartilage. Multizone scaffolds were seeded with human chondrocytes for a long-term *in vitro* culture period of 5 weeks, and biochemical and mechanical analysis were carried at various time points.

MATERIALS AND METHODS

Materials. All materials were purchased from Sigma Aldrich unless otherwise stated.

Scaffold Fabrication. *Printed Helix.* The bottom zone of the multizone scaffold is composed of a cryo-printed helix. The cryo-printed helices were made using 8% w/v polycaprolactone (PCL) in 1,4-dioxane and were printed using a cryo-printer, as described in the previous literature.[28] Briefly, the polymer solution was printed in a helix shape directly onto a cold plate set at −40 °C. The parameters used were as follows: 45 °C print head temperature, 0.5 mm/s print head speed, 1.25 mL/h flow rate of polymer solution, and 18 G needle (0.8 mm in inner diameter). The printed helices were left at −80 °C for 24 h and were freeze-dried (Labconco Freeze-Zone) for 24 h.

Multizone Scaffolds. Electrospinning was employed to fabricate both the middle randomly orientated and the top aligned zones of the multizone scaffolds (Figure 1). The polymer solution consisted of 8% w/v PCL in 1,1,1,3,3,3-hexafluoro-2-propanol (HFIP) (Manchester Organics, UK). First, the middle randomly orientated fibers were electrospun directly onto the cryo-printed helix scaffolds followed by the deposition of the aligned fibers using the parameters detailed in Table 1. The multizone scaffolds were allowed to dry overnight before being cut in 10 mm discs. The multizone scaffolds were made using electrospinning and cryo-printing, in which the porous architecture is obtained via phase separation; thus, electrospun and phase-separated scaffolds were used as controls for the multizone scaffolds. The phase-separated controls were made using 8% w/v PCL in 1,4-dioxane via pouring solutions into molds set at −40 °C on the cold plate, freezing at −80 °C for 24 h, and then freeze-drying for 24 h. The electrospun controls were fabricated with both randomly orientated and aligned fibers using the parameters described in Table 1. The width and height of the scaffolds were 10 mm × 1 mm, 10 mm × 0.5 mm, and 10 mm × 2 mm for the multizone, electrospun, and phase-separated controls, respectively.

Table 1. Electrospinning Parameters for Middle Randomly Orientated and Top Aligned Fibers

parameter	middle random zone	top aligned zone
mandrel rotation (rpm)	200	2400
total volume (mL)	8	5
flow rate (mL/h)	2	2
mandrel-to-needle distance (cm)	11	11
positive charge (kV)	13	13
needle size (gauge)	18	18

Multizone Scaffold Characterization. *Scanning Electron Microscopy.* Morphologies of the multizone, phase-separated control, and electrospun control scaffolds were analyzed using a Hitachi S4700 field emission scanning electron microscope (SEM) (Hitachi) equipped with a 5 kV accelerating voltage. The surface of the scaffolds and internal structure were imaged. Prior to imaging, scaffolds were sputter coated with a thin layer of gold and palladium alloy (Polaron sputter coater).

Fiber Diameter. Fiber diameter and pore size were both evaluated from the SEM images (n = 3) of both the multizone and the controls scaffolds using Image J software (NIH). Fifty measurements from each image were taken, and mean ± standard error of mean was calculated.

Fast Fourier Transform Analysis. Fast Fourier transform (FFT) was performed on SEM images (n = 3) of multizone and control scaffolds to analyze the relative degree of fiber alignment through the conversion of the SEM image into frequency spacing. SEM images were processed using Image J using the oval profile plug-in where FFT images were made and analyzed, as described previously.[45] The radial intensity was summed and plotted with respect to the angle of acquisition.

Pore Circularity Analysis. Pore circularity was also calculated from the SEM images (n = 3) of the printed helix from the multizone scaffold and the phase-separated control using Diameter J plug-in (Image J). The shape of each pore is defined as the degree of circularity, as described previously.[46−48]

Scaffold Preparation and Seeding. *Plasma Coating.* PCL naturally displays hydrophobic characteristics; thus, all scaffolds were plasma coated to make scaffolds more hydrophilic and to improve cell attachment.[49,50] Scaffolds were plasma coated with oxygen, and it has been previously shown to improve hydrophilicity without having an influence in mechanical properties and scaffold morphology.[50] Prior to plasma coating, scaffolds were sterilized in 70% ethanol for 30 min, rinsed thrice in PBS for 15 min each, and freeze-dried overnight. Scaffolds were plasma coated with oxygen using a Harrick Plasma cleaner and PlasmaFlo gas flow mixer (PPC-FMG-2, Harrick Plasma) at 26.6 W (high setting) and 500 mTorr for 3 min. After coating, scaffolds were immediately placed into PBS supplemented with 1% antibiotic/antimycotic before being transferred into 12-well plates with 1.5 mL of chondrocyte growth media (Sigma Aldrich).

Culture of Human Chondrocytes and Multizone Helix Scaffold Seeding. Primary human adult chondrocytes (Sigma, Cell Applications) were cultured in T75 tissue culture flasks using chondrocyte growth media (Sigma Aldrich) according to the manufacturer's instructions. Chondrocytes were cultured to passage five, with twice a week media changes, and were then trypsinized using standard tissue culture methods. A suspension of 100,000 cells in 20 μL was seeded onto each scaffold before being incubated for 3 h to allow cell attachment. Then, 1.5 mL of chondrocyte differentiation media was added to each well (high-glucose DMEM supplemented with 50 μg/mL ascorbic acid, 50 μg/mL L-proline, 0.1 mM sodium pyruvate, 10 ng/mL TGF-β_3 (Biolegend), 1% ITS premix, and 1% antibiotic/antimycotic). For the multizone scaffolds, chondrocytes were seeded directly into the void of the helix zone on the electrospun fibers underneath. Scaffolds were cultured at 37 °C and 5% CO_2 for

https://dx.doi.org/10.1021/acsomega.9b04022
ACS Omega 2020, 5, 12623−12636

24 h and 1, 3, and 5 week time points, with weekly media changes.

Chondrocyte Attachment. Cell attachment was assessed on scaffolds after 24 h of culture using SEM. Chondrocyte-seeded scaffolds were rinsed thrice in PBS before being fixed in 4% v/v glutaraldehyde (Fisher Scientific) in PBS at 4 °C overnight. Scaffolds were then rinsed in PBS three times before and after being post-fixed in 0.1% v/v osmium tetroxide (Electron Microscopy Supplies) in PBS. Scaffolds were dehydrated through an ethanol gradient of 30−100% and were placed in hexamethyldisilazane and allowed to evaporate and dry overnight at room temperature. Scaffolds were coated with gold and palladium alloy before imaging.

Biochemical Characterization. *Cell Viability.* CellTiter-Blue cell viability assay (Promega) was conducted according to the manufacturer's protocol. Briefly, scaffolds (n = 4 per group) were transferred into new wells prior to the addition of CellTiter-Blue working solution (1:5 CellTiter-Blue reagent to media). Scaffolds were incubated for 4 h (37 °C and 5% CO_2). Samples were read using a Modulus II microplate multimode reader at an excitation wavelength of 525 nm and emission wavelength of 580−640 nm.

DNA Analysis. DNA was quantified using a Quant-iT PicoGreen dsDNA Assay Kit (ThermoFisher Scientific) according to the manufacturer's instructions. Briefly, scaffolds (n = 4 per group) were freeze-dried overnight, weighed, and cut in small pieces. Scaffolds were digested in a 2.5 U/mL papain solution containing $CaCl_2$- and $MgCl_2$-free PBS, 5 mM cysteine-HCl, and 5 mM ethylenediaminetetraacetic acid (EDTA) overnight at 60 °C with periodic vortexing. DNA levels in the papain digested samples were measured using the PicoGreen fluorescent dye. The fluorescence intensity was measured at an excitation wavelength of 480 nm and emission wavelength of 510−570 nm using a Modulus II microplate multimode reader.

Glycosaminoglycan Quantification. Glycosaminoglycan (GAG) content was determined using a sulfated GAG assay kit (Blyscan, Biocolor Ltd.) according to the manufacturer's protocol. Papain digested samples were also used for GAG quantification. The absorbance of samples was analyzed using a Modulus II microplate multimode reader at an excitation wavelength of 656 nm. The Sulfated GAG content was obtained using the standard curve.

Fluorescence Seeded Scaffold Imaging. Images of the multizone scaffolds were acquired at each time point. For fluorescence staining, scaffolds were first rinsed three times in PBS and then fixed in 4% formalin in PBS overnight. The scaffolds were then rinsed in PBS before permeabilizing in 0.2% Triton X-100 for 30 min. After 3× 10 min washes in PBS, the cells attached to the scaffold were stained with 1000X phalloidin-iFluorTM514 conjugate (AAT Bioquest, Stratech) in PBS with 1% bovine serum albumin (1:1000) for 1 h. Further 3× 10 min washes were carried out in PBS. Next, the cells were stained with 300 nM 4′,6-diamidino-2-phenylindole (DAPI) in PBS for 10 min. Finally, after 3× 10 min washes in PBS, scaffolds were then mounted on glass coverslips for imaging.

Multiphoton Microscopy. Coherent anti-Stokes Raman scattering (CARS) and two-photon excitation fluorescence (TPEF) images were acquired on a custom-built multiphoton microscope described previously.[51] CARS microscopy was used to image the PCL scaffold fibers (2911 cm^{-1}) whilst simultaneously exciting TPEF from the stained cells (phalloidin and DAPI). The signals were collected in epidetection with the laser excitation separated from the detected signals using a 776 nm dichroic beam splitter and a 785 nm shortpass filter. CARS and phalloidin signals were acquired simultaneously by separating the emission using a dichroic filter cube consisting of a 649 nm dichroic, with 660/13 nm and 542/50 nm bandpass filters, respectively. DAPI images were acquired sequentially using a second filter cube consisting of a 570 nm dichroic beam splitter with a 454/50 nm bandpass filter. All images were acquired using a 25×/1.05 N.A water immersion objective lens (XLPlan N, Olympus) with 75 and 115 mW at the sample for the 1064 and 812.6 nm beams, respectively.

Z-stacks of the multizone scaffolds were acquired to visualize cell growth across the ridge of the helix, with images taken at 2 μm intervals up to 450 μm into the sample. To visualize cell growth across the helix, maximum intensity projection (icy) was used to project all slices onto a single 2D image, which allowed for visualization of the boundary and growth on the inner cell layer. Moreover, images showing the orthogonal view on the Y/Z plane were also constructed (icy) to analyze the cross-sectional location of chondrocytes. To further visualize the location of chondrocytes on the helix scaffold, Z-stacks were compiled to 3D images, and the surface of chondrocytes was rendered.

Widefield Epifluorescence Microscopy. Epifluorescence images of phalloidin stained cells on the multizone scaffold were acquired using an inverted microscope (DMIRB, Leica) with a 5×/0.12 N.A objective lens (N Plan, Leica) and motorized sample stage (Proscan III, Prior). The sample was illuminated by a metal halide lamp (LumenPro 200) with a 485/20 nm excitation bandpass filter. A multiband filter set was used to separate the fluorescence emission from the excitation source (69300, Chroma). Images were acquired using an Andor Zyla sCMOS camera with 60 ms exposure time. The lamp, camera, and motorized sample stage (Prior) were controlled using a micromanager v2.0 to collect a grid of images across the sample with 20% overlap. The individual images were then stitched together using the grid collection stitching plug-in for Fiji to create a large area image of the full scaffold.

Mechanical Properties Analysis. Compressive properties of scaffolds were assessed using an Instron Model 3367 testing machine. Non-seeded scaffolds (n = 4) were soaked in PBS 24 h prior to testing, whereas the seeded scaffolds were immersed in PBS and put in a −80 °C freezer after each time point until testing. All samples were compressed to 30% strain at a crosshead speed of 0.5% strain/min. Young's modulus was calculated from the linear region of the stress−strain curve. Incremental compressive moduli were investigated from 0 to 10%, 10 to 20%, and 20 to 30% strains, as previously described.[11,14]

Reverse Transcription Real-Time Polymerase Chain Reaction (RT-qPCR). RNA was isolated for all scaffolds (n = 3 per group) using 1 mL of TRI reagent (ThermoFisher Scientific). Chloroform (200 μL) was added to the homogenized samples, and RNA was precipitated in 400 μL of ethanol. RNA was purified using Qiagen's RNeasy spin column system, and cDNA was synthesized using Promega's ImProm-II Reverse Transcription System according to the manufacturer's protocol. Quantitative real-time polymerase chain reaction was performed using the LightCycler 480 Instrument II (Roche Life Science) and QuantiNova SYBR

https://dx.doi.org/10.1021/acsomega.9b04022
ACS Omega 2020, 5, 12623−12636

Green PCR Kit (Qiagen). The primers used were collagen I, collagen II, aggrecan, and glyceraldehyde-3-phosphate dehydrogenase (GAPDH), and their sequences are shown in Table 2. Gene expression values were normalized to GAPDH housekeeping gene and were presented as relative expression to 24 h time point scaffolds for each group. The $2^{-\Delta\Delta Ct}$ method was used to calculate relative mRNA levels.

Table 2. Primer Sequences

gene	sequence
collagen 1 (COL1A1)	forward: 5′-GGACACAGAGGTTTCAGTGGT
	reverse: 5′-GCACCATCATTTCCACGAGC
collagen 2 (COL2A1)	forward: 5′-CATCCCACCCTCTCACAGTT
	reverse: 5′-GTCTCTGCCTTGACCCAAAG
aggrecan (ACAN)	forward: 5′-GCTACCCTGACCCTTCATC
	reverse: 5′-AAGCTTTCTGGGATGTCCAC
GAPDH	forward: 5′-GTCTCCTCTGACTTCAACAG
	reverse: 5′-GTTGTCATACCAGGAAATGAG

Statistical Analysis. Results have been presented as mean ± standard error of mean. Statistical analysis was performed using one-way ANOVA with Tukey post hoc test. Statistical significance is marked as $*p < 0.05$, $**p < 0.01$, and $***p < 0.001$.

RESULTS

Multizone Scaffold Characterization. Scaffold morphology was analyzed using SEM, and these SEM images were used to characterize the fiber diameter and pore size of the different zones. Multizone scaffolds comprise three different zones, and as confirmed by the SEM images, each zone expresses distinctive morphology (Figure 2). The bottom helix scaffold has a porous architecture, and the middle and top zones

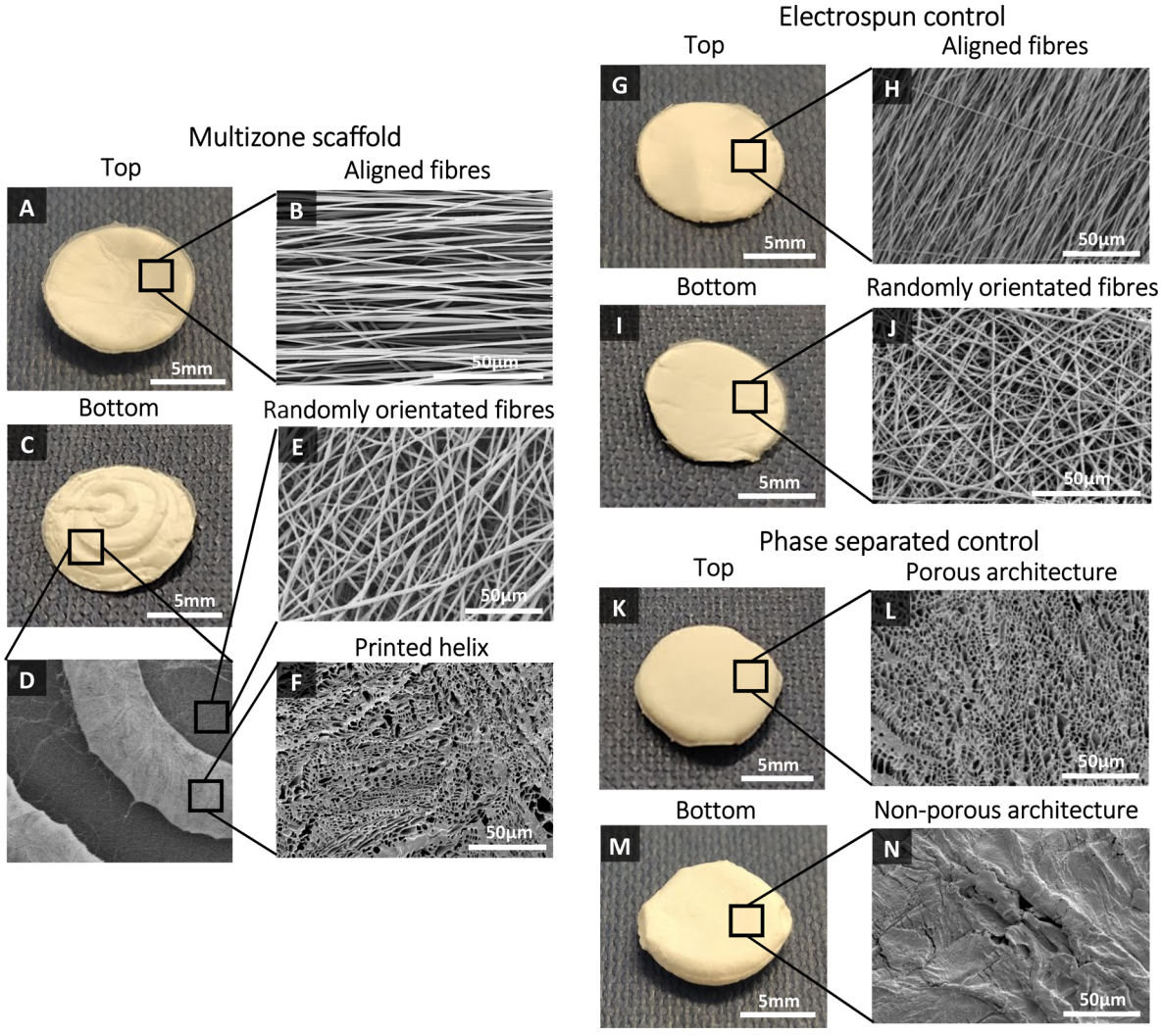

Figure 2. Multizone, phase-separated control, and electrospun control scaffold morphology. Multizone scaffolds: (A) top of the multizone scaffold, (B) SEM image of aligned electrospun fibers in the top layer of the multizone scaffold, (C) bottom of the multizone scaffold, (D) SEM image of the printed helix on top of the electrospun fibers in the multizone scaffold, (E) SEM image of randomly orientated electrospun fibers in the middle layer of the multizone scaffold, and (F) SEM image of porous bottom printed helix of the multizone scaffold. Electrospun control: (G) top of the electrospun control scaffold, (H) SEM image of aligned fibers in the top layer of the electrospun control scaffold, (I) bottom of the electrospun control scaffold, and (J) SEM image of randomly orientated fibers in the bottom layer of the electrospun control scaffold. Phase-separated control: (K) top of the phase-separated control scaffold, (L) SEM image of the porous architecture of the phase-separated control scaffold, (M) bottom of the phase-separated control scaffold, and (N) SEM image of the closed structure on the bottom of the phase-separated control scaffold.

https://dx.doi.org/10.1021/acsomega.9b04022
ACS Omega 2020, 5, 12623−12636

present randomly orientated and aligned fibers, respectively. The aligned fiber diameter in the top layer of the scaffold measured 1.57 ± 0.50 μm, while the randomly orientated fibers in the middle zone had larger diameters at 1.94 ± 0.51 μm. The pore diameter of the helix scaffold was 3.62 ± 2.46 μm (Table 3). The fiber diameter of the electrospun control and the pore size of the phase-separated control are displayed in Table 3. The internal architecture of the scaffold was also analyzed (Figure 3). Successful merging of each distinctive layer of the multizone scaffold (helix, random electrospun fibers, and aligned electrospun fibers) was achieved (Figure 3A). FFT analysis further validated the arrangement of the multizone top aligned electrospun layer and the electrospun control layer and the randomly orientated fibers in the middle layer of the multizone scaffold and the electrospun control. The degree of alignment can be identified as the FFT data exhibit sharp peaks for the aligned fibers and random spikes for the randomly orientated fibers (Figure 4A−D). In the printed helix, 68% of the pores had a high degree of circularity above 0.8. In comparison, the only 57% phase-separated control scaffold pores displayed circularity above 0.8 (Figure 4E,F). The similarity in fiber orientation, fiber size, pore size, and pore circularity between the multizone scaffold and the controls suggests that the phase-separated and electrospun controls used in this study are relevant to form the multizone scaffold.

Table 3. Fibre Diameter and Pore Size Characterization of the Different Zones of the Multizone Scaffold

fiber diameter (μm, mean ± SD)		
multizone scaffold	aligned fibers (top zone)	1.57 ± 0.50
	random fibers (middle zone)	1.94 ± 0.51
electrospun control	aligned fibers (top zone)	1.78 ± 0.38
	random fibers (middle zone)	1.44 ± 0.36
pore size (μm, mean ± SD)		
multizone scaffold	helix scaffold (bottom zone)	3.62 ± 2.46
phase-separated control		4.06 ± 1.91

Cell Attachment and Viability. The ability of human chondrocytes to adhere and proliferate on scaffolds was evaluated over 5 weeks of culture. Multizone scaffolds displayed significantly greater cell attachment compared to both phase-separated and electrospun controls, as shown in the 24 h CellTiter-Blue viability results (Figure 5A). Moreover, cell viability was maintained over a long 5 week culture period, with significantly higher cell viability being noted in the multizone scaffolds after 24 h and 1 and 5 weeks of culture compared to both phase-separated and electrospun control groups. PicoGreen DNA quantification further demonstrated long-term cell attachment and survival over 5 weeks of culture, with a similar DNA quantity between the groups at all time points (Figure 5B).

Sulfated Glycosaminoglycan Synthesis. The GAG content was detected at each time point using a sulfated GAG detection kit. GAG production displayed an increasing trend over 5 weeks of culture with significant increased levels of GAG after 3 and 5 weeks of culture in all groups (Figure 6).

Fluorescence Staining. Images captured using CARS and TPEF of chondrocytes, stained with DAPI (nuclei) and phalloidin (actin filaments), confirm the presence of cells on all scaffolds after 5 weeks of culture (Figure 7). Images displayed in Figure 7 represent localized chondrocyte attachment on scaffolds. In order to investigate localization of cells on the multizone scaffold, epifluorescence imaging was conducted. As demonstrated by the epifluorescence image in Figure 1, the chondrocytes are localized in the void of the helix zone directly on the electrospun fibers of the middle zone. Chondrocyte attachment on the multizone scaffolds was further investigated through Z projections, 2D cross-sectional views, and 3D rendering (Figure 8). It is highlighted that the chondrocytes attach to the electrospun fibers under the helix zone. Moreover, these images confirm the cell viability and DNA content results as they show the presence of cells on the scaffolds.

Mechanical Properties. Incremental compressive properties were calculated for non-seeded and seeded scaffolds over 5 weeks of culture, and results are presented in Figure 9. First, for non-seeded scaffolds, the phase-separated control scaffolds presented relatively high compressive properties in comparison to the electrospun control and multizone scaffolds for all strain increments 0−10, 10−20, and 20−30%. Multizone scaffolds displayed slightly higher, but not significant, compressive properties to the electrospun control scaffolds. Moreover, the compressive properties did not vary over the 4 week culture period and was similar to the acellular controls at all strains; however, only data between 0 and 30% strain is presented.

Expression of Cartilage-Specific ECM Genes. The expression of key chondrocyte genes was investigated over 5 weeks of culture. Figure 10 displays specific gene expression for

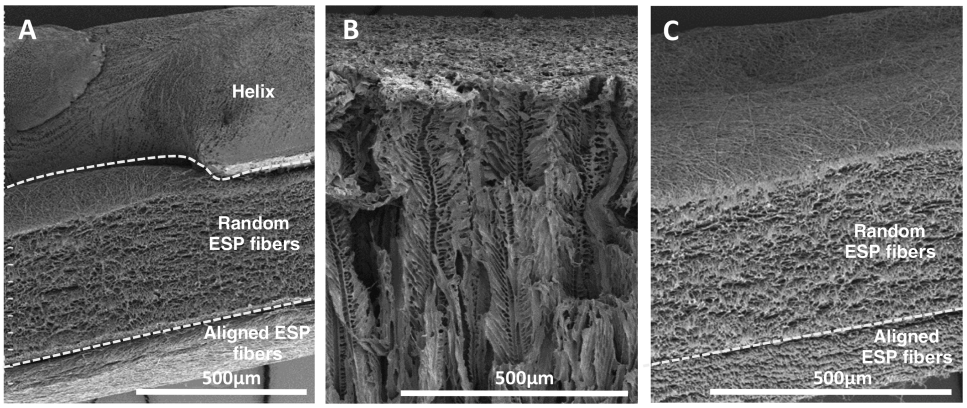

Figure 3. Side view of scaffolds to show the internal architecture of the (A) multizone scaffold, (B) phase-separated control scaffold, and (C) electrospun control scaffold.

https://dx.doi.org/10.1021/acsomega.9b04022
ACS Omega 2020, 5, 12623−12636

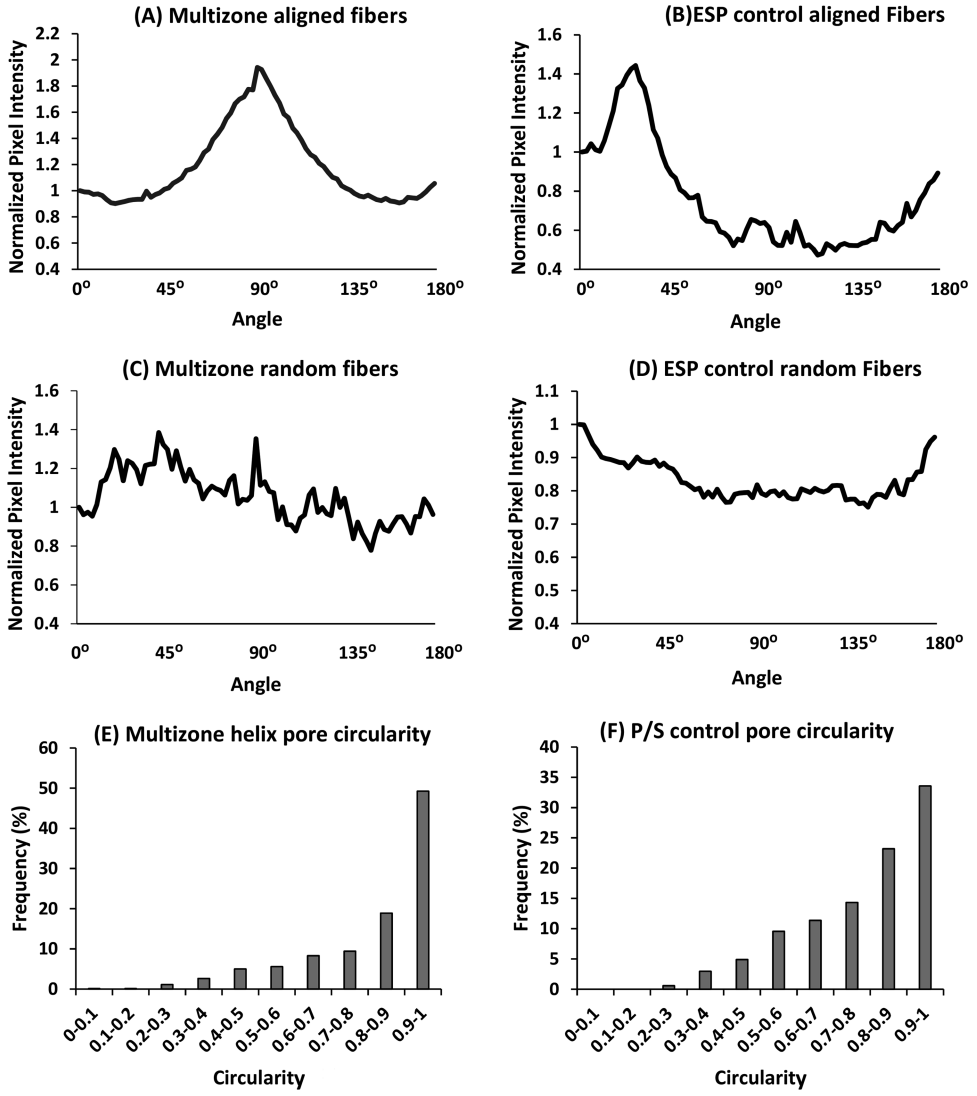

Figure 4. Multizone, phase-separated control, and electrospun control scaffold morphology characterization. Fast Fourier transform analysis was performed to investigate the degree of fiber alignment on (A) aligned fibers on the multizone scaffold, (B) aligned fibers on the ESP control scaffold, (C) randomly orientated fibers on the multizone scaffold, and (D) randomly orientated fibers on the ESP control scaffold. Pore circularity of the (E) printed helix layer of the multizone scaffold and (F) P/S control scaffold. P/S: phase-separated control; ESP: electrospun control.

the multizone scaffolds and both phase-separated and electrospun control scaffolds. Both collagen II (COL2A1) and aggrecan (ACAN) expression was significantly upregulated in the multizone scaffolds over 5 weeks of culture. A significant increase in collagen I (COL1A1) was also noted for the multizone scaffolds, but this was only evident between 24 h and 5 week time points. Phase-separated control scaffolds failed to display the expression of chondrogenic genes collagen II and aggrecan. Electrospun control scaffolds revealed an increasing trend in collagen II expression; however, this was not significant.

DISCUSSION

The present study successfully demonstrates the ability of multizone scaffolds to support chondrocyte adherence, growth, and differentiation. These scaffolds were made using PCL, which has been previously used to develop a number of FDA-approved medical devices.[52] Combining the use of cryo-printing and electrospinning allowed the fabrication of multizone scaffolds that possessed high porosity and controlled architectures that are relevant to the native cartilage. While the cryo-printed helix provides the necessary interconnected architecture and compressive support, the electrospun layers provide an ECM-like environment that influences cell attachment and growth.

The key aim of the multizone scaffolds fabricated in this study was to mimic the transition of collagen orientation in the three zones of the native cartilage: deep, middle, and superficial zones. The deep zone of the native cartilage displays a perpendicular arrangement of the collagen fibers, which is responsible for providing the greatest resistance to compressive forces.[53] Directional freezing is a well-established technique to produce scaffolds with a columnar structure, which displays a similar arrangement as the deep zone.[37,54−56] Moreover, previous studies have incorporated bioactive factors within directionally frozen scaffolds to achieve adequate cell growth and mechanical properties.[14,57] In the present study, the use of cryo-printing allowed successful mimicking of the columnar structure of the deep zone and the ability to print a helix structure. Cryo-printing is a computer-aided manufacturing

https://dx.doi.org/10.1021/acsomega.9b04022
ACS Omega 2020, 5, 12623−12636

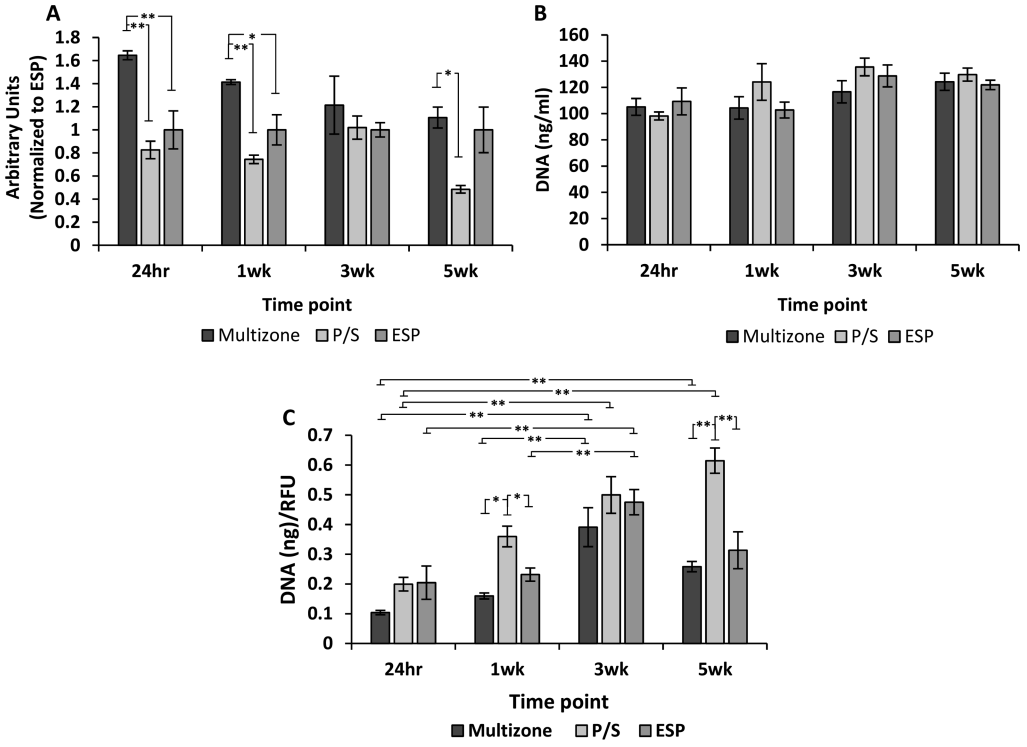

Figure 5. Biochemical evaluation of scaffolds over 5 weeks of culture. (A) Cell viability assessed through CellTiter-Blue assay. The fluorescence is normalized to the electrospun control scaffolds at 24 h. (B) DNA quantification measured using PicoGreen assay. (C) DNA normalized to cell viability. Error bars = standard error mean, $n = 4$. Statistical significance denoted by $^{*}p < 0.05$, $^{**}p < 0.01$; one-way ANOVA with Tukey post hoc test. P/S: phase-separated control; ESP: electrospun control.

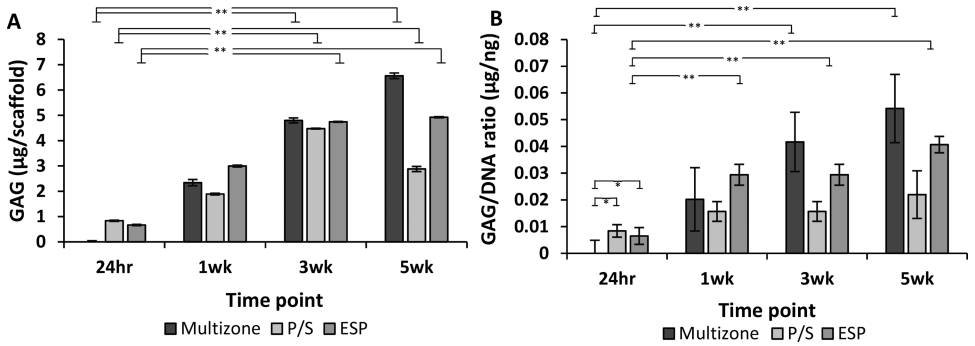

Figure 6. Sulfated glycosaminoglycan synthesis over 5 weeks of culture. (A) Sulfated glycosaminoglycan content. (B) Sulfated glycosaminoglycan content normalized to DNA. Error bars = standard error mean, $n = 4$. Statistical significance denoted by $^{*}p < 0.05$, $^{**}p < 0.01$; one-way ANOVA with Tukey post hoc test. P/S: phase-separated control; ESP: electrospun control.

process that combines 3D printing with directional freezing, and it allows printing of desired shapes with high porosity.[28] Previously, cryo-printing has been employed to produce highly controllable porous and interconnected scaffolds composed of both macro- and nanopores for bone and cartilage applications.[28,29,58−62]

Over the years, electrospinning has proven to be economical and efficient in creating fibrous meshes with the ability to replicate both the structure and function of the ECM in various tissue engineering applications.[10,50,63] In the present study, the random orientation of the electrospun fibers, in the middle layer of the multizone scaffold, reproduces the oblique arrangement of the collagen fibers in the middle zone of the native cartilage.[53] Moreover, the aligned organization of the top layer represents the superficial zone of the native cartilage. The superficial zone, which is composed of tightly packed aligned collagen fibers and flattened chondrocytes, is responsible for frictionless gliding, tensile properties, and protecting other zones from shear stresses. A previous study has presented the ability of aligned electrospun fibers to direct cell growth and, interestingly, to possess low friction properties.[42] Moreover, the addition of aligned fibers on particulate template scaffolds reduced surface roughness due to the densely packed fibres,[11] suggesting that the use of aligned fibers is favorable to mimic the low frictional characteristics of the native cartilage.

Cell attachment and proliferation during *in vitro* assessment is of importance as it determines the biocompatibility of the scaffold. Multizone scaffolds displayed improved cell attachment compared to the phase-separated and electrospun controls. This was further confirmed by cell nuclei and actin filament staining, which shows a difference in the number of

https://dx.doi.org/10.1021/acsomega.9b04022
ACS Omega 2020, 5, 12623−12636

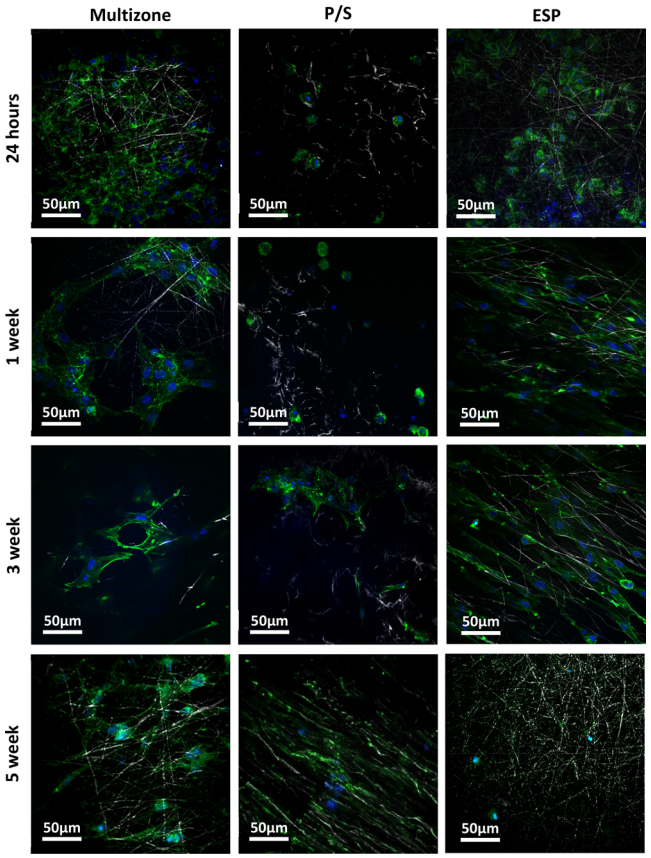

Figure 7. Two-photon excitation fluorescence (TPEF) and coherent anti-Stokes Raman scattering (CARS) images of chondrocytes attached on multizone, phase-separated, and electrospun scaffolds over 5 weeks of culture. P/S: phase-separated control; ESP: electrospun control.

attached cell between the groups at 24 h as shown in Figure 7. This may be attributed to the helix structure adopted for the bottom layer of the multizone scaffold. The printed helix allowed increased seeding efficiency as the void permits the cells to be seeded into the large pore, while the electrospun layers under the printed helix act as a sieve, entrapping the cells. Moreover, the orthogonal, 2D cross-sectional view in Figure 8 of the multizone scaffold clearly shows that the chondrocytes are localized on the electrospun fibers. Although no changes in DNA content was noted between the multizone and controls scaffolds over 5 weeks of culture, cell viability was higher in the multizone scaffolds compared to the controls (Figure 5). The DNA quantification method, PicoGreen, provides accurate DNA quantification;[64] however, its accuracy in some 3D structures is limited due to the fact it accounts for DNA of dead cells, which are trapped within the scaffold porous architecture. Thus, no change in DNA may be noted in this present study. Furthermore, as would be expected, there is no direct correlation between cell viability and DNA content.

Large pore sizes and adequate interconnectivity are thought to facilitate cellular infiltration, growth, and nutrient transport, while small pores are required to allow enough surface area to allow cell attachment.[63] Pore sizes ranging between 60 and 200 μm have supported cartilage production in a porcine model and chondrogenesis.[65−69] Previous studies have also shown that gradients in pore size are favorable for the stimulation of chondrogenesis; however, some studies presented the lack of cellular infiltration to the deep layers of the scaffolds, questioning their ability to fully regenerate tissues.[10,22,39] Multizone scaffolds presented a gradient in pore size with the bottom helix layer presenting macro- and microscale pores and the electrospinning zone displaying varied pore sizes.

Chondrocytes play a great role in the development and maintenance of the cartilage through the synthesis of various matrix components. Collagen is the most abundant structural macromolecule, accounting for 60% of dry weight of the cartilage, followed by proteoglycans, which account for 10−15%.[41,53] A significant upregulation of both collagen II (COL2A1) and aggrecan (ACAN) was revealed in the multizone scaffolds over time (Figure 10) as well as increased levels of proteoglycans, measured through sulfated GAG content (Figure 6). Collagen II and aggrecan are the most predominant type of collagen and proteoglycan found in the native cartilage. Their increased expression of these scaffolds in the multizone scaffolds over 5 weeks of culture shows that chondrocytes are expressing the relevant phenotypic markers. Phase-separated control scaffolds failed to express both collagen II and aggrecan genes; however, the expression of collagen I was noted. The increased expression of collagen I indicates the differentiation of chondrocytes where they lose phenotypic properties. The electrospun control displayed the unaltered expression of collagen I and aggrecan over a 5 week culture period; however, a non-significant but increasing trend in collagen II was noted. This suggests that the combination of both these techniques to capture the zonal architecture of the native cartilage allows the successful regulation of key gene expression. For future work, it is necessary to further validate the production of ECM molecules including collagen and aggrecan via immunohistochemical staining. Nonetheless, multizone scaffolds have shown the potential as platforms that successfully influence key gene expression.

Implantation of scaffolds depends on the use of autologous chondrocytes that are isolated from a small biopsy of the cartilage and grown *in vitro* to achieve an adequate number of cells for scaffold seeding. Expansion of chondrocytes *in vitro* significantly affects the phenotypic mechanisms of cultured chondrocytes.[70] Moreover, over time, chondrocytes lose their differentiated phenotype and the ability to express cartilage-specific components including collagen II and aggrecan. Previously, many strategies including culturing cells in pellets or polymer gels and the addition of FBS to culture media promoted chondrocyte redifferentiation;[70] however, in the present study, serum-free culture media were utilized, and cells were expanded in a monolayer. ACI involves the use of *in vitro* expanded chondrocytes to ensure that an adequate number of cells are obtained for implantation; however, this procedure leads to the differentiation of chondrocytes. The current method for obtaining relevant chondrocyte numbers for implantation in techniques including ACI utilizes a high number of doublings, and a similar level was employed in this study, aligning with clinical procedures,[43,44] rather than using a lower doubling number, which is often employed in other studies. In this study, the multizone scaffolds demonstrated to facilitate redifferentiation as shown by a significant increase in both collagen II and aggrecan gene expression after 5 weeks of culture. Although the chondrocytes differentiation media were supplemented with TGF-β_3, which provides appropriate biochemical cues for differentiation, both control groups failed to express the relevant genes.[71] This suggests that the multizone scaffold promotes redifferentiation of chondrocytes,

https://dx.doi.org/10.1021/acsomega.9b04022
ACS Omega 2020, 5, 12623−12636

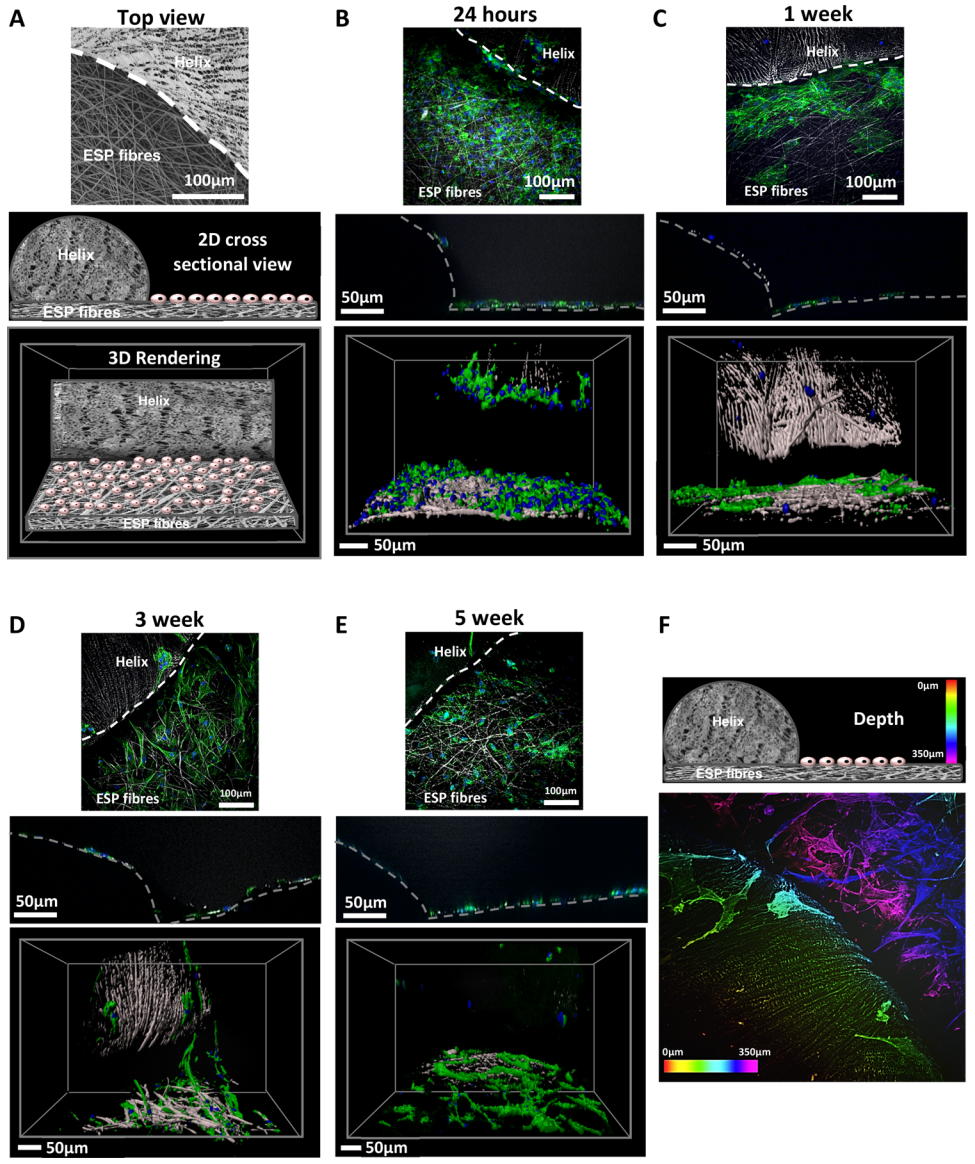

Figure 8. Two-photon excitation fluorescence (TPEF) and coherent anti-Stokes Raman scattering (CARS) Z stack, 2D cross-sectional, and 3D rendering images of chondrocytes attached on multizone over 5 weeks of culture. Blue indicates DAPI (nuclei) staining, and green represents phalloidin (actin filaments) staining. (A) SEM image of the stop view of scaffolds and illustration of 2D cross section and 3D rendering of chondrocytes on multizone scaffolds. Z stack, 2D cross section, and 3D rendering images of chondrocytes attached on multizone at (B) 24 h, (C) 1 week, (D) 3 weeks, and (E) 5 weeks. (F) Z stack of the multizone scaffold showing color-dependent depth.

and this may be attributed to the bottom helix scaffold, which successfully allowed cells to be seeded at a high density into a large pore, improving cell-to-cell interactions. Both high-density scaffold seeding and cell-to-cell interactions have been previously reported to promote redifferentiation of chondrocytes. Moreover, after 5 weeks of culture, although the chondrocytes adopt a fibroblast-like morphology, they still possess relevant gene expression.

Mechanical properties of constructs for cartilage tissue engineering is of great importance as the articular cartilage facilitates the transmission of loads and has an excellent ability to endure high cyclic loads. Structural and compositional variations between zones are responsible for the capability of the cartilage to withstand complex and combined loads.[37,72] Compressive properties of scaffolds have been shown to be dependent on pore alignment,[73] and the influence of pore alignment on mechanical properties has been previously reported in bone and cartilage applications.[74] The phase-separated control scaffold in this present study presented to possess relatively high compressive properties in comparison to the native cartilage, whereas electrospun controls expressed low properties.[37] The bottom helix layer of the multizone scaffold is responsible for the compressive properties, and interestingly, adopting a helix shape allows reduction of the compressive properties of the multizone scaffold in comparison to the phase-separated control.

While this study has presented the potential of multizone scaffolds over a 5 week culture period, further work is required to fully evaluate the capability of these scaffolds to support chondrogenesis. Although *in vitro* study results advocate the initial promise of the scaffold to support cell attachment and cell survival, further *in vivo* investigation is of importance to ensure translatability and the maintenance of chondrogenic phenotype. It is also essential to investigate how the scaffold

https://dx.doi.org/10.1021/acsomega.9b04022
ACS Omega 2020, 5, 12623−12636

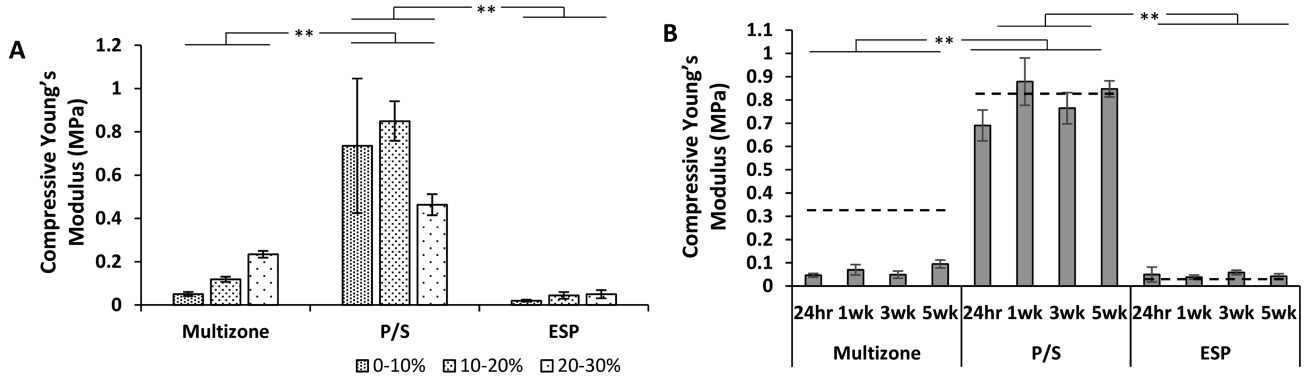

Figure 9. Compressive Young's Modulus of (A) non-seeded scaffolds between 1−10, 10−20, and 20−30% strains and (B) chondrocyte-seeded scaffolds between 0 and 30% strain over 5 weeks of culture. Dashed line represents compressive Young's Modulus of non-seeded scaffold between 0 and 30% strain. Error bars = standard error mean, $n = 3$. Statistical significance denoted by $*p < 0.05$, $**p < 0.01$; one-way ANOVA with Tukey post hoc test. P/S: phase-separated control; ESP: electrospun control.

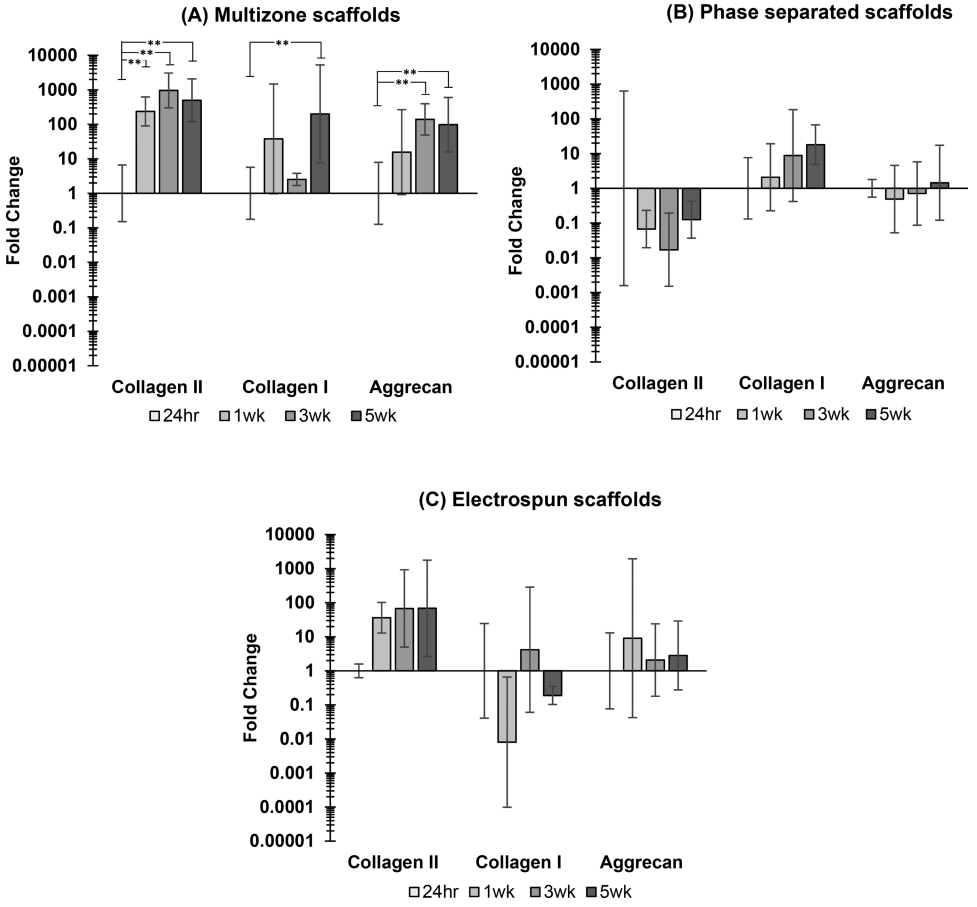

Figure 10. Gene expression of (A) multizone scaffolds, (B) phase-separated control scaffolds, and (C) electrospun control scaffolds. Values normalized to GAPDH housekeeping gene and are relative to 24 h time point gene expression for each group. Relative expression is calculated using the $2^{-\Delta\Delta Ct}$ method. Error bars = standard error mean, $n = 3$. Statistical significance denoted by $*p < 0.05$, $**p < 0.01$; one-way ANOVA with Tukey post hoc test

will integrate biomechanically into a cartilage lesion with a mineral base and poroelastic sidewalls. The scaffolds were robust, and no delamination was noted during this 5 week *in vitro* study; however, it is vital for future studies to investigate delamination under shear stresses and in *in vivo* models. Nevertheless, this study provides initial findings, which indicate the potential of multizone scaffolds in cartilage tissue engineering.

CONCLUSIONS

Multizone scaffolds developed using various fabrication techniques in this study not only successfully recapitulate the complex collagen fiber orientation of the native cartilage but also possess relevant compressive properties. This zonal organization of the scaffold allowed for cell attachment, production of the major ECM component, GAG, and effective regulation of key gene expression over a 5 week culture period.

https://dx.doi.org/10.1021/acsomega.9b04022
ACS Omega 2020, 5, 12623−12636

All these factors suggest the potential of multizone scaffolds in the field of cartilage tissue engineering. Additionally, various ECM molecules or biological cues can be incorporated into the surface of the scaffolds in order to create bioactive multizone scaffolds, which capture both the structure and ECM component into the scaffold.

AUTHOR INFORMATION

Corresponding Author

Anthony Callanan − *School of Engineering, Institute for Bioengineering, University of Edinburgh, Edinburgh EH9 3JL, Scotland;* orcid.org/0000-0002-1871-2853; Phone: +44(0)131 6507355; Email: Anthony.Callanan@ed.ac.uk

Authors

Nimrah Munir − *School of Engineering, Institute for Bioengineering, University of Edinburgh, Edinburgh EH9 3JL, Scotland*

Alison McDonald − *School of Engineering, Institute for Bioengineering, University of Edinburgh, Edinburgh EH9 3JL, Scotland*

Complete contact information is available at: https://pubs.acs.org/10.1021/acsomega.9b04022

Notes

The authors declare no competing financial interest.

ACKNOWLEDGMENTS

The authors would like to thank Prof. Alistair Elfick for use of lab facilities (IBioE, University of Edinburgh) and Steve Mitchell for imaging assistance (BioSEM, University of Edinburgh). We would also like to thank the IMPACT imaging facility (Centre for Discovery Brain Sciences, University of Edinburgh) for allowing us access to the IMARIS image analysis software and Dr. Marta Mikolajczak for assistance. This work is funded by an Engineering & Physical Sciences Research Council [EPSRC] Doctoral Training Partnership Studentship UK, Regenerative Medicine Platform II [RMPII] grant MR/L022974/1 and the MRC computational and chemical biology of the stem cell niche grant (CCBN) MR/L012766/1.

REFERENCES

(1) Hunziker, E. B. Articular Cartilage Repair: Basic Science and Clinical Progress. A Review of the Current Status and Prospects. *Osteoarthr. Cartil.* **2002**, *10*, 432−463.

(2) Mintz, B. R.; Cooper, J. A., Jr. Hybrid Hyaluronic Acid Hydrogel/Poly(ε-Caprolactone) Scaffold Provides Mechanically Favorable Platform for Cartilage Tissue Engineering Studies. *J. Biomed. Mater. Res. - Part A* **2014**, *102*, 2918−2926.

(3) Amadori, S.; Torricelli, P.; Panzavolta, S.; Parrilli, A.; Fini, M.; Bigi, A. Multi-Layered Scaffolds for Osteochondral Tissue Engineering: In Vitro Response of Co-Cultured Human Mesenchymal Stem Cells. *Macromol. Biosci.* **2015**, *15*, 1535−1545.

(4) Zhang, Y.; Jordan, J. M. Epidemiology of Osteoarthritis. *Clin. Geriatr. Med.* **2010**, *26*, 355−369.

(5) Johnson, V. L.; Hunter, D. J. The Epidemiology of Osteoarthritis. *Best Pract. Res. Clin. Rheumatol.* **2014**, *28*, 5−15.

(6) McGowan, K. B.; Stiegman, G. Regulatory Challenges for Cartilage Repair Technologies. *Cartilage* **2013**, *4*, 4−11.

(7) Liu, S.; Wu, J.; Liu, X.; Chen, D.; Bowlin, G. L.; Cao, L.; Lu, J.; Li, F.; Mo, X.; Fan, C. Osteochondral Regeneration Using an Oriented Nanofiber Yarn-Collagen Type I/Hyaluronate Hybrid/TCP Biphasic Scaffold. *J. Biomed. Mater. Res. A* **2015**, 581−592.

(8) Peck, Y.; He, P.; Chilla, G. S. V. N.; Poh, C. L.; Wang, D.-A. A Preclinical Evaluation of an Autologous Living Hyaline-like Cartilaginous Graft for Articular Cartilage Repair : A Pilot Study. *Sci. Rep.* **2015**, *5*, 1−14.

(9) Kessler, M. W.; Grande, D. A. Tissue engineering and cartilage. *Organogenesis* **2014**, *4*, 28−32.

(10) McCullen, S. D.; Autefage, H.; Callanan, A.; Gentleman, E.; Stevens, M. M. Anisotropic Fibrous Scaffolds for Articular Cartilage Regeneration. *Tissue Eng. Part A* **2012**, *18*, 2073−2083.

(11) Steele, J. A. M.; McCullen, S. D.; Callanan, A.; Autefage, H.; Accardi, M. A.; Dini, D.; Stevens, M. M. Combinatorial Scaffold Morphologies for Zonal Articular Cartilage Engineering. *Acta Biomater.* **2014**, *10*, 2065−2075.

(12) Zhang, J.; Wu, Y.; Thote, T.; Lee, E. H.; Ge, Z.; Yang, Z. The Influence of Scaffold Microstructure on Chondrogenic Differentiation of Mesenchymal Stem Cells. *Biomed. Mater.* **2014**, *9*, No. 035011.

(13) Kwon, H.; Sun, L.; Cairns, D. M.; Rainbow, R. S.; Preda, R. C.; Kaplan, D. L.; Zeng, L. The influence of scaffold material on chondrocytes under inflammatory conditions. *Acta biomaterialia* **2013**, *9*, 6563−6575.

(14) Munir, N.; Callanan, A. Novel Phase Separated Polycaprolactone/Collagen Scaffolds for Cartilage Tissue Engineering. *Biomed. Mater.* **2018**, *13*, No. 051001.

(15) Reid, J. A.; Callanan, A. Hybrid Cardiovascular Sourced Extracellular Matrix Scaffolds as Possible Platforms for Vascular Tissue Engineering. *J. Biomed. Mater. Res. Part B Appl. Biomater.* **2019**, *108*, 910−924.

(16) Grant, R.; Hay, D.; Callanan, A. From Scaffold to Structure: The Synthetic Production of Cell Derived Extracellular Matrix for Liver Tissue Engineering. *Biomed. Phys. Eng. Express* **2018**, *4*, No. 065015.

(17) Reid, J. A.; Callanan, A. Influence of Aorta Extracellular Matrix in Electrospun Polycaprolactone Scaffolds. *J. Appl. Polym. Sci.* **2019**, *136*, 48181.

(18) Burton, T. P.; Callanan, A. A Non-woven Path: Electrospun Poly(lactic acid) Scaffolds for Kidney Tissue Engineering. *J. Tissue Eng. Regen. Med.* **2018**, *15*, 301−310.

(19) Chung, S.; Gentilini, C.; Callanan, A.; Hedegaard, M.; Hassing, S.; Stevens, M. M. Responsive Poly (γ-Glutamic Acid) Fibres for Biomedical Applications. *J. Mater. Chem. B* **2013**, *1*, 1397−1401.

(20) Shalumon, K. T.; Binulal, N. S.; Selvamurugan, N.; Nair, S. V.; Menon, D.; Furuike, T.; Tamura, H.; Jayakumar, R. Electrospinning of Carboxymethyl Chitin/Poly(Vinyl Alcohol) Nanofibrous Scaffolds for Tissue Engineering Applications. *Carbohydr. Polym.* **2009**, *77*, 863−869.

(21) Nandakumar, A.; Barradas, A.; de Boer, J.; Moroni, L.; van Blitterswijk, C.; Habibovic, P. Combining Technologies to Create Bioactive Hybrid Scaffolds for Bone Tissue Engineering. *Biomatter* **2013**, *3*, 1−13.

(22) Garrigues, N. W.; Little, D.; Sanchez-Adams, J.; Ruch, D. S.; Guilak, F. Electrospun Cartilage-Derived Matrix Scaffolds for Cartilage Tissue Engineering. *J. Biomed. Mater. Res. - Part A* **2014**, *102*, 3998−4008.

(23) Grant, R.; Hallett, J.; Forbes, S.; Hay, D.; Callanan, A. Blended Electrospinning with Human Liver Extracellular Matrix for Engineering New Hepatic Microenvironments. *Sci. Rep.* **2019**, *9*, 6293.

(24) Grant, R.; Hay, D. C.; Callanan, A. A Drug-Induced Hybrid Electrospun Poly-Capro-Lactone: Cell-Derived Extracellular Matrix Scaffold for Liver Tissue Engineering. *Tissue Eng. Part A* **2017**, *23*, 650−662.

(25) Zhou, Y.; Chyu, J.; Zumwalt, M. Recent Progress of Fabrication of Cell Scaffold by Electrospinning Technique for Articular Cartilage Tissue Engineering. *Int. J. Biomater.* **2018**, *2018*, 1.

(26) Xu, T.; Binder, K. W.; Albanna, M. Z.; Dice, D.; Zhao, W.; Yoo, J. J.; Atala, A. Hybrid Printing of Mechanically and Biologically Improved Constructs for Cartilage Tissue Engineering Applications. *Biofabrication* **2013**, *5*, No. 015001.

(27) Moroni, L.; Schotel, R.; Hamann, D.; de Wijn, J. R.; van Blitterswijk, C. A. 3D Fiber-Deposited Electrospun Integrated Scaffolds Enhance Cartilage Tissue Formation. *Adv. Funct. Mater.* **2008**, *18*, 53−60.
(28) Munir, N.; Larsen, R. S.; Callanan, A. Fabrication of 3D Cryo-Printed Scaffolds Using Low-Temperature Deposition Manufacturing for Cartilage Tissue Engineering. *Bioprinting* **2018**, *10*, No. e00033.
(29) Munir, N.; McDonald, A.; Callanan, A. A Combinatorial Approach: Cryo-Printing and Electrospinning Hybrid Scaffolds for Cartilage Tissue Engineering. *Bioprinting* **2019**, *16*, No. e00056.
(30) Ahn, S.; Kim, Y.; Lee, H.; Kim, G. A New Hybrid Scaffold Constructed of Solid Freeform-Fabricated PCL Struts and Collagen Struts for Bone Tissue Regeneration: Fabrication, Mechanical Properties, and Cellular Activity. *J. Mater. Chem.* **2012**, *22*, 15901.
(31) Kim, G.; Son, J.; Park, S.; Kim, W. Hybrid Process for Fabricating 3D Hierarchical Scaffolds Combining Rapid Prototyping and Electrospinning. *Macromol. Rapid Commun.* **2008**, *29*, 1577−1581.
(32) Centola, M.; Rainer, A.; Spadaccio, C.; De Porcellinis, S.; Genovese, J. A.; Trombetta, M. Combining Electrospinning and Fused Deposition Modeling for the Fabrication of a Hybrid Vascular Graft. *Biofabrication* **2010**, *2*, No. 014102.
(33) Chen, R.; Morsi, Y.; Patel, S.; Ke, Q.-f.; Mo, X.-m. A Novel Approach via Combination of Electrospinning and FDM for Tri-Leaflet Heart Valve Scaffold Fabrication. *Front. Mater. Sci. China* **2009**, *3*, 359−366.
(34) Klein, T. J.; Malda, J.; Sah, R. L.; Hutmacher, D. W. Tissue Engineering of Articular Cartilage with Biomimetic Zones. *Tissue Eng. Part B. Rev.* **2009**, *15*, 143−157.
(35) Levingstone, T. J.; Matsiko, A.; Dickson, G. R.; O'Brien, F. J.; Gleeson, J. P. A Biomimetic Multi-Layered Collagen-Based Scaffold for Osteochondral Repair. *Acta Biomater.* **2014**, *10*, 1996−2004.
(36) Kim, T.-K.; Sharma, B.; Williams, C. G.; Ruffner, M. A.; Malik, A.; McFarland, E. G.; Elisseeff, J. H. Experimental Model for Cartilage Tissue Engineering to Regenerate the Zonal Organization of Articular Cartilage. *Osteoarthr. Cartil.* **2003**, *11*, 653−664.
(37) Arora, A.; Kothari, A.; Katti, D. S. Pore Orientation Mediated Control of Mechanical Behavior of Scaffolds and Its Application in Cartilage-Mimetic Scaffold Design. *J. Mech. Behav. Biomed. Mater.* **2015**, *51*, 169−183.
(38) Reed, S.; Lau, G.; Delattre, B.; Lopez, D. D.; Tomsia, A. P.; Wu, B. M. Macro- and Micro-Designed Chitosan-Alginate Scaffold Architecture by Three-Dimensional Printing and Directional Freezing. *Biofabrication* **2016**, *8*, 1−16.
(39) Woodfield, T. B. F.; Malda, J.; De Wijn, J.; Péters, F.; Riesle, J.; Van Blitterswijk, C. A. Design of Porous Scaffolds for Cartilage Tissue Engineering Using a Three-Dimensional Fiber-Deposition Technique. *Biomaterials* **2004**, *25*, 4149−4161.
(40) Woodfield, T. B. F.; Van Blitterswijk, C. A.; De Wijn, J.; Sims, T. J.; Hollander, A. P.; Riesle, J. Polymer Scaffolds Fabricated with Pore-Size Gradients as a Model for Studying the Zonal Organization within Tissue-Engineered Cartilage Constructs. *Tissue Eng.* **2005**, *11*, 1297−1311.
(41) Delcroix, G. J.-R.; Molinari, M.; Reiner, T.; Temple, H. T.; Valdes, M.; Montero, R. B.; Andreopoulos, F. M.; Schiller, P. C.; D'Ippolito, G. Multi-Layered Scaffold to Mimic Hyaline Articular Cartilage Architecture. *Curr. Tissue Eng.* **2016**, *5*, 21−28.
(42) Accardi, M. A.; McCullen, S. D.; Callanan, A.; Chung, S.; Cann, P. M.; Stevens, M. M.; Dini, D. Effects of Fiber Orientation on the Frictional Properties and Damage of Regenerative Articular Cartilage Surfaces. *Tissue Eng. Part A* **2013**, *19*, 2300−2310.
(43) Brittberg, M.; Lindahl, A.; Nilsson, A.; Ohlsson, C.; Isaksson, O.; Peterson, L. Treatment of Deep Cartilage Defects in the Knee with Autologous Chondrocyte Transplantation. *N. Engl. J. Med.* **1994**, *331*, 889−895.
(44) Viste, A.; Piperno, M.; Desmarchelier, R.; Grosclaude, S.; Moyen, B.; Fessy, M. H. Autologous Chondrocyte Implantation for Traumatic Full-Thickness Cartilage Defects of the Knee in 14 Patients: 6-Year Functional Outcomes. *Orthop. Traumatol. Surg. Res.* **2012**, *98*, 737−743.
(45) Huang, C.-Y.; Hu, K.-H.; Wei, Z.-H. Comparison of Cell Behavior on Pva/Pva-Gelatin Electrospun Nanofibers with Random and Aligned Configuration. *Sci. Rep.* **2016**, *6*, 37960.
(46) Khodaei, M.; Meratian, M.; Savabi, O.; Razavi, M. The Effect of Pore Structure on the Mechanical Properties of Titanium Scaffolds. *Mater. Lett.* **2016**, *171*, 308−311.
(47) Mazzuca, E.; Salito, C.; Rivolta, I.; Aliverti, A.; Miserocchi, G. From Morphological Heterogeneity at Alveolar Level to the Overall Mechanical Lung Behavior: An in Vivo Microscopic Imaging Study. *Physiol. Rep.* **2014**, *2*, e00221.
(48) Bakalova, L. P.; Andreasen, C. M.; Thomsen, J. S.; Brüel, A.; Hauge, E.-M.; Kiil, B. J.; Delaisse, J.-M.; Andersen, T. L.; Kersh, M. E. Relating Intracortical Bone Mechanics to Pore Morphology and Remodeling Characteristics in the Human Fibula. *J. Bone Miner. Res.* **2018**, *33*, 2177.
(49) Abbasi, N.; Soudi, S.; Hayati-Roodbari, N.; Dodel, M.; Soleimani, M. The Effects of Plasma Treated Electrospun Nanofibrous Poly (ε-Caprolactone) Scaffolds with Different Orientations on Mouse Embryonic Stem Cell Proliferation. *Cell J.* **2014**, *16*, 245−254.
(50) Burton, T. P.; Corcoran, A.; Callanan, A. The Effect of Electrospun Polycaprolactone Scaffold Morphology on Human Kidney Epithelial Cells. *Biomed. Mater.* **2018**, *13*, 1−14.
(51) Downes, A.; Mouras, R.; Elfick, A. A Versatile CARS Microscope for Biological Imaging. *J. Raman Spectrosc.* **2009**, *40*, 757−762.
(52) Woodruff, M. A.; Hutmacher, D. W. The Return of a Forgotten Polymer—Polycaprolactone in the 21st Century. *Prog. Polym. Sci.* **2010**, *35*, 1217−1256.
(53) Sophia Fox, A. J.; Bedi, A.; Rodeo, S. A. The Basic Science of Articular Cartilage: Structure, Composition, and Function. *Sports Health* **2009**, *1*, 461−468.
(54) Pot, M. W.; Faraj, K. A.; Adawy, A.; van Enckevort, W. J. P.; van Moerkerk, H. T. B.; Vlieg, E.; Daamen, W. F.; van Kuppevelt, T. H. Versatile Wedge-Based System for the Construction of Unidirectional Collagen Scaffolds by Directional Freezing: Practical and Theoretical Considerations. *ACS Appl. Mater. Interfaces* **2015**, *7*, 8495−8505.
(55) Rowland, C. R.; Colucci, L. A.; Guilak, F. Fabrication of Anatomically-Shaped Cartilage Constructs Using Decellularized Cartilage-Derived Matrix Scaffolds. *Biomaterials* **2016**, *91*, 57−72.
(56) Dunphy, S. E.; Reid, J. A.; Burton, T. P.; Callanan, A. Mechanical Characterisation of Directionally Frozen Polycaprolactone Scaffolds Using 1, 4-Dioxane and Glacial Acetic Acid for Articular Cartilage Tissue Engineering. *Biomed. Phys. Eng. Express* **2018**, *4*, 057004.
(57) Guan, J.; Stankus, J. J.; Wagner, W. R. Development of Composite Porous Scaffolds Based on Collagen and Biodegradable Poly(Ester Urethane)Urea. *Cell Transpl.* **2017**, *15*, 17−27.
(58) Liao, C.-Y.; Wu, W.-J.; Hsieh, C.-T.; Tseng, C.-S.; Dai, N.-T.; Hsu, S. Design and Development of a Novel Frozen-Form Additive Manufacturing System for Tissue Engineering Applications. *3D Print. Addit. Manuf.* **2016**, *3*, 216−225.
(59) Liu, L.; Xiong, Z.; Zhang, R.; Jin, L.; Yan, Y. A Novel Osteochondral Scaffold Fabricated via Multi-Nozzle Low-Temperature Deposition Manufacturing. *J. Bioact. Compat. Polym.* **2009**, *24*, 18−30.
(60) Pham, C. B.; Leong, K. F.; Lim, T. C.; Chian, K. S. Rapid Freeze Prototyping Technique in Bio-Plotters for Tissue Scaffold Fabrication. *Rapid Prototyp. J.* **2008**, *14*, 246−253.
(61) Xiong, Z.; Yan, Y.; Wang, S.; Zhang, R.; Zhang, C. Fabrication of Porous Scaffolds for Bone Tissue Engineering via Low-Temperature Deposition. *Scr. Mater.* **2002**, *46*, 771−776.
(62) Yen, H.-J.; Hsu, S.-H.; Tseng, C.-S.; Huang, J.-P.; Tsai, C.-L. Fabrication of Precision Scaffolds Using Liquid-Frozen Deposition Manufacturing for Cartilage Tissue Engineering. *Tissue Eng. Part A* **2009**, *15*, 965−975.

https://dx.doi.org/10.1021/acsomega.9b04022
ACS Omega 2020, 5, 12623−12636

(63) Pham, Q. P.; Sharma, U.; Mikos, A. G. Electrospun Poly (ε -Caprolactone) Microfiber and Multilayer Nanofiber/Microfiber Scaffolds: Characterization of Scaffolds and Measurement of Cellular Infiltration. *Biomacromolecules* **2006**, *7*, 2796−2805.
(64) Singer, V. L.; Jones, L. J.; Yue, S. T.; Haugland, R. P. Characterization of PicoGreen Reagent and Development of a Fluorescence-Based Solution Assay for Double-Stranded DNA Quantitation. *Anal. Biochem.* **1997**, *249*, 228−238.
(65) Cai, R.; Nakamoto, T.; Kawazoe, N.; Chen, G. Influence of Stepwise Chondrogenesis-Mimicking 3D Extracellular Matrix on Chondrogenic Differentiation of Mesenchymal Stem Cells. *Biomaterials* **2015**, *52*, 199−207.
(66) Callanan, A.; Davis, N. F.; McGloughlin, T. M.; Walsh, M. T. The Effects of Stent Interaction on Porcine Urinary Bladder Matrix Employed as Stent-Graft Materials. *J. Biomech.* **2014**, *47*, 1885−1893.
(67) Enea, D.; Cecconi, S.; Calcagno, S.; Busilacchi, A.; Manzotti, S.; Gigante, A. One-Step Cartilage Repair in the Knee: Collagen-Covered Microfracture and Autologous Bone Marrow Concentrate. A Pilot Study. *Knee* **2015**, *22*, 30−35.
(68) Stenhamre, H.; Nannmark, U.; Lindahl, A.; Gatenholm, P.; Brittberg, M. Influence of Pore Size on the Redifferentiation Potential of Human Articular Chondrocytes in Poly(Urethane Urea) Scaffolds. *J. Tissue Eng. Regen. Med.* **2011**, *5*, 578−588.
(69) Xia, W.; Liu, W.; Cui, L.; Liu, Y.; Zhong, W.; Liu, D.; Wu, J.; Chua, K.; Cao, Y. Tissue Engineering of Cartilage with the Use of Chitosan-Gelatin Complex Scaffolds. *J. Biomed. Mater. Res. - Part B Appl. Biomater.* **2004**, *71B*, 373−380.
(70) Chen, G.; Sato, T.; Ushida, T.; Hirochika, R.; Tateishi, T. Redifferentiation of Dedifferentiated Bovine Chondrocytes When Cultured in Vitro in a PLGA-Collagen Hybrid Mesh. *FEBS Lett.* **2003**, *542*, 95−99.
(71) Barry, F.; Boynton, R. E.; Liu, B.; Murphy, J. M. Chondrogenic Differentiation of Mesenchymal Stem Cells from Bone Marrow: Differentiation-Dependent Gene Expression of Matrix Components. *Exp. Cell Res.* **2001**, *268*, 189−200.
(72) Jeuken, R. M.; Roth, A. K.; Peters, R. J. R. W.; van Donkelaar, C. C.; Thies, J. C.; van Rhijn, L. W.; Emans, P. J. Polymers in Cartilage Defect Repair of the Knee: Current Status and Future Prospects. *Polymer* **2016**, *8*, 1−30.
(73) Wu, X.; Liu, Y.; Li, X.; Wen, P.; Zhang, Y.; Long, Y.; Wang, X.; Guo, Y.; Xing, F.; Gao, J. Preparation of Aligned Porous Gelatin Scaffolds by Unidirectional Freeze-Drying Method. *Acta Biomater.* **2010**, *6*, 1167−1177.
(74) Deville, S.; Saiz, E.; Tomsia, A. P. Freeze Casting of Hydroxyapatite Scaffolds for Bone Tissue Engineering. *Biomaterials* **2006**, *27*, 5480−5489.

https://dx.doi.org/10.1021/acsomega.9b04022
ACS Omega 2020, 5, 12623−12636